

PDE-CONSTRAINED OPTIMIZATION MODELS AND PSEUDOSPECTRAL METHODS FOR MULTISCALE PARTICLE DYNAMICS

MILDRED ADUAMOAH*, BENJAMIN D. GODDARD†, JOHN W. PEARSON‡, AND
JONNA C. RODEN§

Abstract. We derive novel algorithms for optimization problems constrained by partial differential equations describing multiscale particle dynamics, including non-local integral terms representing interactions between particles. In particular, we investigate problems where the control acts as an advection ‘flow’ vector or a source term of the partial differential equation, and the constraint is equipped with boundary conditions of Dirichlet or no-flux type. After deriving continuous first-order optimality conditions for such problems, we solve the resulting systems by developing a link with computational methods for statistical mechanics, deriving pseudospectral methods in both space and time variables, and utilizing variants of existing fixed point methods. Numerical experiments indicate the effectiveness of our approach for a range of problem set-ups, boundary conditions, as well as regularization and model parameters.

Key words. PDE-constrained optimization; Multiscale particle dynamics; Pseudospectral methods

AMS subject classifications. 35Q70, 35Q93, 49J20, 65N35, 82C22

1. Introduction. In this work we describe a novel approach for tackling optimization problems for systems in which the underlying dynamics are described by multiscale, interacting particle systems. Our methods are widely applicable to the optimization of many systems described by non-local, non-linear partial differential equations (PDEs), some cases of which have recently received attention in the literature [2, 3, 5, 12, 14, 25]. The principal novelties are a link to state-of-the-art methods in statistical mechanics (known as Dynamic Density Functional Theory, or DDFt) [22, 29, 45, 48, 58, 68, 69], the implementation of a pseudospectral method, both in space and time, allowing highly efficient and accurate solution of both the forward and optimization problems [13, 65], and a modification of existing ‘sweeping’, or fixed point, algorithms [3, 16] to increase the stability for the problems studied here. We also demonstrate how to efficiently implement Neumann (no-flux) boundary conditions, provide a number of exact and validation test cases, and accompany the paper with an open source software implementation [1], based on 2DChebClass [35, 51]. Our use of pseudospectral methods has three main advantages over existing implementations: (i) due to a novel implementation of spatial convolutions, we are not restricted to periodic domains or the use of Fourier grids; (ii) for problems of the types studied here, where the solutions are expected to be smooth and we require accurate solutions, pseudospectral methods provide significant computational gains over finite difference or finite element approaches; (iii) using pseudospectral interpolation in time allows one to move beyond fixed timestepping methods, and implement more accurate

*School of Mathematics and Maxwell Institute for Mathematical Sciences, The University of Edinburgh, Edinburgh, EH9 3FD, UK (maduamoa@ed.ac.uk)

†School of Mathematics and Maxwell Institute for Mathematical Sciences, The University of Edinburgh, Edinburgh, EH9 3FD, UK (b.goddard@ed.ac.uk)

‡School of Mathematics and Maxwell Institute for Mathematical Sciences, The University of Edinburgh, Edinburgh, EH9 3FD, UK (j.pearson@ed.ac.uk)

§School of Mathematics and Maxwell Institute for Mathematical Sciences, The University of Edinburgh, Edinburgh, EH9 3FD, UK (J.C.Roden@sms.ed.ac.uk)

and efficient ordinary differential equation (ODE) and differential–algebraic equation (DAE) solvers.

This paper is structured as follows. In Section 2 we provide relevant background to multiscale particle dynamics, pseudospectral methods, and PDE-constrained optimization (PDECO). In Section 3 we give the associated first-order optimality conditions, followed by a description of the numerical methods in Section 4. The results of our numerical experiments are reported in Section 5, followed by some concluding remarks in Section 6.

2. Background. In this section we detail the necessary background required for the development of our algorithms. In Section 2.1 we describe relevant material on multiscale particle dynamics, in Section 2.2 we outline pseudospectral methods, in Section 2.3 we state the PDE-constrained optimization problems of particle dynamics problems that we will consider, and in Section 2.4 we survey related work in the area of mean-field optimal control.

2.1. Multiscale particle dynamics. The dynamics of many systems can be accurately described by interacting particles or agents. Examples range in scale from electrons in atoms and molecules [63], through biological cells in tissues [8], up to planets and stars in galaxies [11]. Other individual-based models include animals undergoing flocking and swarming [70], pedestrians walking [26], or people who interact and thus change their opinions [44].

In principle, such situations can be modelled by differential equations for the ‘state’ (e.g., position, momentum, opinion) of each individual. However, the challenge here is that physical systems typically have huge numbers of particles (e.g., $\sim 10^{25}$ molecules in a litre of water) and, as such, are beyond the treatment of standard numerical methods, both in terms of storage and processor time. For N particles, typical algorithms scale as N^2 or N^3 , which prevents direct computation for more than, say, $\mathcal{O}(10^4)$ particles. It is clear from the vast separation of scales between computationally tractable and physically relevant problems that this issue cannot be overcome through the sequential improvement of computer hardware.

An additional complication of directly solving the dynamics of such systems, e.g., through Newtonian dynamics, is the sensitive dependence on initial conditions [43]. For many physical systems, it is unreasonable to assume that one knows the exact initial conditions for each particle. As such, one is interested not in a particular realization of the dynamics, but rather in an ‘average’ behaviour, which is typical for the system.

Both of these challenges suggest that it would be prudent to instead study the dynamics through a statistical mechanics approach, for which one is interested in the macroscopic quantities, rather than individual realizations [38]. However, this approach comes with its own challenges and drawbacks.

The first is that, at least without additional simplifying approximations, the resulting equations are no easier to solve than the underlying particle dynamics. For example, instead of treating the Langevin stochastic differential equation (SDE), which formally scales computationally as N^2 , one may treat the corresponding Fokker–Planck (forward Kolmogorov/Smoluchowski) equation, which is a partial differential equation (PDE) in dN dimensions, where d is the number of degrees of freedom of the one-particle phase space (typically 6 when including momentum, and 3 when only considering the particle positions). A standard approach would then be to discretize each degree of freedom, reducing the PDE to a system of coupled ODEs, which may

then, in principle, be solved numerically. The issue here lies with the curse of dimensionality: for M points in each degree of freedom, one requires a total of M^{dN} points. Taking, for the sake of argument, $M = 10$ points and $N = 10$ particles in three dimensions, then the total number of points required is 10^{30} , which is far too many for a reasonable computation, and far too few for an accurate solution.

A common approach to overcome this is to use ‘coarse-graining’, which reduces the dimensionality of the system, generally at the cost of a loss of accuracy or physical effects, and the introduction of unconstrained approximations [67]. This links to the second challenge, which concerns the multiscale nature of the problem. In many systems of interest, physically crucial effects manifest themselves on scales of the particle size, all the way up to the macroscale. Examples include volume exclusion of hard particles [15], biological cellular alignment [10], and nucleation of clusters and clouds [46]. A standard coarse-graining approach would be to ignore effects such as volume exclusion, and treat the whole system as a bulk, and hence determine quantities such as average densities and orientations [38]. Whilst this is viable in homogeneous systems close to equilibrium, it completely fails to capture heterogeneous systems, symmetry breaking, and many dynamical effects.

However, an extremely efficient and accurate example of coarse-graining which captures such effects is Dynamic Density Functional Theory (DDFT) [22, 48]. The crucial observation here is that the full N -body information in a system is a functional of the 1-body density, $\rho(\vec{x}, t)$ (i.e., the probability of finding any one particle at a given position at a given time). This is an extension of classical density functional theory (DFT) (see, e.g., the early works [29, 58] and later reviews [45, 68, 69]), which considers the equilibrium case, and is linked to the celebrated quantum version [37]. The main challenge here is that the proof is non-constructive; it is unknown how to map from ρ to the full information in the system. However, in many practical applications, it is ρ itself that is the quantity of interest. Hence it is desirable to derive closed equations of motion for the 1-body density, which is an object in \mathbb{R}^d , irrespective of N .

The simplest example is the diffusion equation, which corresponds to Brownian motion, and concerns non-interacting particles; here the reduction to the 1-body density is trivial. We are instead concerned with systems in which the particles interact, e.g., through electrostatic forces, volume exclusion, or exchange of information. Typical DDFTs can be thought of as generalized diffusion equations of the form

$$\partial_t \rho(\vec{x}, t) = \nabla \cdot \left(\rho \nabla \frac{\delta \mathcal{F}[\rho]}{\delta \rho} \right) = -\nabla \cdot \vec{j}. \quad (2.1)$$

Here \mathcal{F} is the Helmholtz free energy of the system. For the non-interacting case, at equilibrium, it is given by

$$\mathcal{F}_{\text{id}}[\rho] = \int \rho(\vec{x}) (\log \rho(\vec{x}) - 1) \, d\vec{x},$$

from which it follows that $\nabla \frac{\delta \mathcal{F}_{\text{id}}[\rho]}{\delta \rho} = \frac{\nabla \rho}{\rho}$, resulting in the diffusion equation.

For more general systems, the exact free energy is unknown (except in the special case of hard rods in one dimension [64]). As such, much effort has been devoted to determine accurate approximations of the free energy for a wide range of systems, but particular focus is given to hard spheres [59] and particles with soft interactions [36]; these cases may be combined in a perturbative manner [30]. Here we will focus on a relatively simple DDFT, which closes the equation for ρ by considering that the particles are, on average, uncorrelated. For particles which interact through an even

pairwise potential V_2 , in an external potential field V_1 , the (approximate) free energy is modelled by

$$\mathcal{F}[\rho] = \int \rho(\vec{x})(\log \rho(\vec{x}) - 1) \, d\vec{x} + \int V_1(\vec{x})\rho(\vec{x}) \, d\vec{x} + \frac{1}{2} \int \int \rho(\vec{x})\rho(\vec{x}')V_2(|\vec{x} - \vec{x}'|) \, d\vec{x}d\vec{x}'.$$

This is known as the *mean-field approximation*, which has been shown to be surprisingly accurate for a range of systems [9], and is known to be exact in the limit of dense systems of particles with soft interactions [50]. We note that this should be considered as the first stepping stone on a path to treat PDE-constrained optimal control systems for general DDFTs. Such systems are highly challenging, not only due to the non-local, non-linear nature of the PDEs, but also due to the complexity of the free energy functionals. For example, Fundamental Measure Theory (FMT), which describes the interactions of systems of hard particles, requires the computation of weighted densities through convolution integrals, followed by a further integral of a complicated function of these weighted densities [59]. As such, these challenges are postponed to future work.

A final challenge we will address here is the implementation of (spatial) boundary conditions. Most physical systems are constrained in some way, often in a ‘box’ with impassable walls, such that the number of particles is conserved. For DDFTs, the corresponding boundary condition is $\vec{j} \cdot \vec{n} = 0$ on the boundary, where \vec{j} is the flux, as in (2.1) and \vec{n} is the unit normal to the boundary. Whilst this is a standard Neumann boundary condition, we note that the difficulty lies in the form of \vec{j} ; for interacting problems, \vec{j} is non-local and, as such, so is the corresponding boundary condition. This results in an equation which is challenging to solve numerically; see Section 4.

2.2. Pseudospectral methods. There are a number of standard methods for solving DDFT-like problems. The two most common are the finite element method (FEM) and pseudospectral methods. Here we focus on the latter, but note that the algorithm presented below (see Section 4) is general and may be easily adapted to other numerical methods. The main challenge in using FEM for DDFT problems lies in their non-locality. Heuristically, the principal benefits of FEM are that it (i) produces large, but sparse matrices, leading to systems which may be efficiently solved, for example through the implementation of standard timestepping schemes and carefully-chosen preconditioners (see e.g., [49, 52, 53, 57, 61, 71] for PDE-constrained optimization problems); and (ii) may be applied to complex domains through standard triangulation/meshing routines. In contrast, for non-local problems such as DDFT the corresponding matrices are not only large, but also dense. This prevents the use of standard numerical schemes and significantly increases the computational cost.

Recently, accurate and efficient pseudospectral methods have been developed to tackle these non-local, non-linear DDFTs [51]. Some details of the implementation will be discussed in Section 4; here we highlight the benefits and challenges. As is widely known [13, 65], pseudospectral methods are extremely accurate for problems with smooth solutions on ‘nice’ domains; here ‘nice’ roughly corresponds to domains which may be mapped to the unit square in a simple (e.g., conformal) manner. They are more challenging to apply on complex domains (although spectral elements can be seen as a compromise between FEM and pseudospectral methods [13]), and are also of poor accuracy when the solutions are not smooth (heuristically, the accuracy is order $(1/N)^p$ where the solution is p -times differentiable, but still at the cost of dense matrices).

Their use to treat DDFT problems stems from three main observations: (i) at

least in principle, the diffusion term present in all DDFTs should lead to smoothing of solutions for sufficiently smooth particle interactions; (ii) the pseudospectral matrices are always dense and, as such, treating non-local terms does not formally affect the numerical cost; (iii) the implementation of non-local boundary conditions may be treated via standard algebraic–differential equations solvers, thus removing the need for bespoke treatments of different boundary conditions.

2.3. PDE-constrained optimization. In this section we introduce the two main PDE-constrained optimization problem structures that we consider within a multiscale particle dynamics setting. A significant additional complication compared to a standard PDE-constrained optimization problem is the addition of an integral, interaction term. In the following, the terms ‘flow control’ and ‘source control’ refer to the application of the control in the PDE constraint either non-linearly, as a vector field within an advection operator, or linearly, as a scalar source term in the PDE.

2.3.1. Flow control problem. We commence with the following problem involving minimizing a cost functional containing a sum of L^2 -norm terms within the entire space-time interval $\Omega \times (0, T)$, constrained by a non-linear time-dependent advection–diffusion equation with additional non-local integral term. The control is applied non-linearly in the form of a vector ‘flow’ term:

$$\begin{aligned} \min_{\rho, \vec{w}} \quad & \mathcal{J}(\rho, \vec{w}) := \frac{1}{2} \int_0^T \int_{\Omega} (\rho - \hat{\rho})^2 \, dxdt + \frac{\beta}{2} \int_0^T \int_{\Omega} \|\vec{w}\|^2 \, dxdt \\ \text{s.t.} \quad & \mathcal{D}(\rho, \vec{w}) - \nabla_r \cdot \mathcal{I}(\rho) = f \quad \text{on } \Omega \times (0, T), \\ & \rho = \rho_0(\vec{x}) \quad \text{at } t = 0, \end{aligned} \tag{2.2}$$

where

$$\mathcal{D}(\rho, \vec{w}) = \partial_t \rho - \nabla^2 \rho + \nabla \cdot (\rho \vec{w}) - \nabla \cdot (\rho \nabla V_{\text{ext}}), \quad \mathcal{I}(\rho) = \kappa \int_{\Omega} \rho(r) \rho(r') \vec{K}(r, r') \, dr'.$$

Here, $\Omega \subset \mathbb{R}^d$, $d \in \{1, 2, 3\}$, is some given domain with boundary $\partial\Omega$, and T is a prescribed ‘final time’ up to which the process is modelled. The scalar function ρ and the vector-valued function \vec{w} are the *state* and *control variables*, respectively, $\beta > 0$ is a given *regularization parameter*, and $\hat{\rho}(\vec{x}, t)$, $V_{\text{ext}}(\vec{x}, t)$, $f(\vec{x}, t)$, $\rho_0(\vec{x})$ are prescribed functions corresponding to the *desired state*, *external potential*, PDE source term, and initial condition, respectively. We highlight that frequently $f(\vec{x}, t) = 0$, which results in conservation of mass; one reason we allow the case $f(\vec{x}, t) \neq 0$ is to enable us to more readily construct analytic test problems for (2.2). Additionally, the non-local integral term models interactions between individual particles, where \vec{K} denotes some vector function. We are particularly interested in the case where \vec{K} is odd, i.e., $\vec{K}(r, r') = -\vec{K}(r', r)$; this is the case when $\vec{K}(r, r') = \nabla_r V_2(r - r')$ with $V_2(\vec{x}) = V_2(\|\vec{x}\|)$ an even potential. However, for now we present the results for a general \vec{K} . For $V_2(\|\vec{x}\|)$ decreasing as $\|\vec{x}\| \rightarrow \infty$, the integral term models repulsive (attractive) interactions when κ is positive (negative). Of course, much more general choices of V_2 are possible. The parameter κ models the particle interaction strength. If κ is set to zero, the model reduces to a standard non-linear advection–diffusion equation control problem.

We consider two possibilities for the boundary conditions imposed on ρ , specifically the Dirichlet boundary condition:

$$\rho = c \quad \text{on } \partial\Omega \times (0, T), \tag{2.3}$$

for a given constant $c \in \mathbb{R}$, and that of the ‘no-flux type’ boundary condition:

$$\mathcal{N}(\rho, \vec{w}) + \mathcal{I}(\rho) \cdot \vec{n} = 0 \quad \text{on } \partial\Omega \times (0, T), \quad (2.4)$$

where

$$\mathcal{N}(\rho, \vec{w}) = \frac{\partial \rho}{\partial n} - \rho \vec{w} \cdot \vec{n} + \rho \frac{\partial V_{\text{ext}}}{\partial n},$$

with $\frac{\partial}{\partial n}$ denoting the derivative with respect to the normal \vec{n} . The latter is a no-flux boundary condition in the classical sense if $f = 0$.

2.3.2. Source control problem. We also consider the following problem, with an analogous cost functional to the flow control problem, but now with a scalar function for the control variable, which is applied linearly in the form of a PDE source term. This is again minimized subject to a non-linear time-dependent advection–diffusion equation with an additional integral term:

$$\begin{aligned} \min_{\rho, w} \quad \mathcal{J}(\rho, w) &= \frac{1}{2} \int_0^T \int_{\Omega} (\rho - \hat{\rho})^2 \, dx dt + \frac{\beta}{2} \int_0^T \int_{\Omega} w^2 \, dx dt \\ \text{s.t.} \quad \mathcal{D}_l(\rho, w) - \nabla_r \cdot \mathcal{I}(\rho) &= f \quad \text{on } \Omega \times (0, T), \\ \rho &= \rho_0(\vec{x}) \quad \text{at } t = 0, \end{aligned} \quad (2.5)$$

where

$$\mathcal{D}_l(\rho, w) = \partial_t \rho - \nabla^2 \rho - \nabla \cdot (\rho \nabla V_{\text{ext}}) - w.$$

This is posed along with the Dirichlet boundary condition (2.3), or the ‘no-flux type’ boundary condition:

$$\mathcal{N}_l(\rho) + \mathcal{I}(\rho) \cdot \vec{n} = 0 \quad \text{on } \partial\Omega \times (0, T), \quad (2.6)$$

where

$$\mathcal{N}_l(\rho) = \frac{\partial \rho}{\partial n} + \rho \frac{\partial V_{\text{ext}}}{\partial n}.$$

2.4. Mean-field optimal control. Mean-field games were first introduced by Lasry and Lions, [39, 40, 41, 42], and independently by Huang, Caines and Malhamé [47], under the name Nash certainty equivalence, and have been widely studied since then. The main challenge over typical PDECO problems arises from the additional non-linear, non-local interaction term. Therefore, standard results in optimal control theory cannot readily be applied, and new approaches have to be developed to address theoretical and numerical challenges.

The most commonly studied controls are through the flow, e.g., [3], interaction term, e.g., [33], or external agents, e.g., [17]. A common assumption is that the particle distribution has compact support [17, 18, 32], which eliminates the need for boundary conditions. No-flux boundary conditions, which are a principal focus of our work, have been considered in limited settings [3, 20].

The two main avenues of research focus on Vlasov-type PDEs arising from the mean-field limit of Cucker–Smale-like [27, 28] models of flocking, and Fokker–Planck equations from the same limit of Langevin dynamics.

For the former, Fornasier et al. provided theoretical results on the convergence of the microscopic sparse optimal control problem to a corresponding macroscopic

problem, using methods of optimal transport and a Γ -limit argument, proving existence of optimal controls in the mean-field setting, see [32, 33, 34]. Additional work on sparse control strategies can be found in [54], as well as in the review paper [31]. In [18], convergence results are proved for systems in which the control is applied through interacting, external agents. For the Fokker–Planck case, analytical research has focused on the derivation of first-order optimality conditions [3], existence and regularity of optimal controls [21], and convergence of the microscopic optimal control problem to the mean-field limit [20, 55].

In terms of numerical implementations, Strang splitting schemes [23, 62] are commonly used, in particular for control strategies which employ external agents [17, 19, 55], in which the numerical results are used to verify convergence in the mean-field limit. In [6], different selective control strategies were considered, and an iterative numerical method was chosen, where the interaction term is approximated stochastically. Other approaches involve combining a Chang–Cooper scheme for the forward equation, finite differences for the adjoint equation, and Monte-Carlo integration [3] to solve the PDEs. The optimization step was performed with a sweeping algorithm, with updates through the gradient equation, which is similar to the gradient descent method in [16]. Other related numerical work applies to porous media Fokker–Planck equations [20], as well as the determination of steady state solutions [4, 7].

As described in Section 4, we will use an optimization scheme that is inspired by existing sweeping algorithms [3, 16], but with a novel coupling to pseudospectral methods used to discretize both the space and time domains. This composition of methods offers an efficient and accurate solver for a wide class of problems. To our knowledge, it is the first time that pseudospectral methods have been applied to non-local optimal control problems of this form.

3. Particle Dynamics Models and First-Order Optimality Conditions.

In this section we derive the system of PDEs that we need to solve in order to tackle the models (2.2) and (2.5). In order to obtain first-order optimality conditions for (2.2) and (2.5), we apply an *optimize-then-discretize method*, meaning we derive appropriate conditions on the continuous level and then consider suitable discretization strategies. The alternative to this approach is the *discretize-then-optimize* method, however we select the former in order to obtain numerical solutions that better reflect the solutions to the continuous first-order optimality conditions. We highlight that an area of active interest in the PDE-constrained optimization community is to construct discretization schemes such that the two approaches coincide (see [24] for a fundamental example of a problem for which different results are obtained using the two methods).

In order to break down the problem into its individual components, and for brevity of exposition, we initially consider the PDE-constrained optimization problem in its traditional form, i.e., without additional integral term $\nabla_r \cdot \mathcal{I}(\rho, \vec{w})$, or equivalently with $\kappa = 0$. We briefly describe how the first-order optimality conditions are formed, for both flow control and source control problems with different boundary conditions, and refer to [66], for instance, for a rigorous justification of how such conditions are formed. To conclude the section, we summarize the first-order optimality conditions for all problems, with $\kappa \neq 0$.

3.1. Flow control with Dirichlet boundary condition. We first consider the advection–diffusion constrained optimization problem (2.2) with the Dirichlet boundary condition (2.3). As mentioned, we initially exclude the interaction term

(so set $\kappa = 0$), for readability. This leads to the continuous Lagrangian:

$$\mathcal{L}(\rho, \vec{w}, q_1, q_2) = \mathcal{J}(\rho, \vec{w}) - \int_0^T \int_{\Omega} (\mathcal{D}(\rho, \vec{w}) - f) q_1 \, dxdt - \int_0^T \int_{\partial\Omega} (\rho - c) q_2 \, dsdt, \quad (3.1)$$

where q_1 and q_2 correspond to the portions of the *adjoint variable* q arising in the interior of the spatial domain Ω and its boundary $\partial\Omega$, respectively.

To obtain first-order optimality conditions, we first follow standard working for deriving the *adjoint equation* for time-dependent PDE-constrained optimization, see [66, Chapter 3] for instance. We obtain that the derivative of \mathcal{L} in the direction ρ must satisfy $D_{\rho}\mathcal{L}(\bar{\rho}, \bar{w}, q_1, q_2)\rho = 0$ for all ρ such that $\rho(\vec{x}, 0) = 0$. Now, from (3.1),

$$D_{\rho}\mathcal{L}(\bar{\rho}, \bar{w}, q_1, q_2)\rho = \int_0^T \int_{\Omega} (\bar{\rho} - \hat{\rho})\rho \, dxdt - \int_0^T \int_{\Omega} \mathcal{D}(\rho, \bar{w})q_1 \, dxdt - \int_0^T \int_{\partial\Omega} \rho q_2 \, dsdt,$$

whereupon by integrating by parts and applying Green's formula, any sufficiently smooth ρ such that $\rho(\vec{x}, 0) = 0$ satisfies

$$\begin{aligned} 0 &= - \int_0^T \int_{\Omega} (-\partial_t q_1 - \nabla^2 q_1 - \bar{w} \cdot \nabla q_1 + \nabla V_{\text{ext}} \cdot \nabla q_1 + \hat{\rho} - \bar{\rho})\rho \, dxdt \\ &\quad + \int_0^T \int_{\Omega} [\nabla \cdot (q_1 \nabla \rho) - \nabla \cdot (\rho \nabla q_1) - \nabla \cdot (\rho q_1 \bar{w}) + \nabla \cdot (\rho q_1 \nabla V_{\text{ext}})] \, dxdt \\ &\quad + \int_{\Omega} q_1(\vec{x}, T)\rho(\vec{x}, T) \, dx - \int_0^T \int_{\partial\Omega} q_2 \rho \, dsdt \\ &= - \int_0^T \int_{\Omega} (-\partial_t q_1 - \nabla^2 q_1 - \bar{w} \cdot \nabla q_1 + \nabla V_{\text{ext}} \cdot \nabla q_1 + \hat{\rho} - \bar{\rho})\rho \, dxdt \\ &\quad + \int_{\Omega} q_1(\vec{x}, T)\rho(\vec{x}, T) \, dx + \int_0^T \int_{\partial\Omega} q_1 \frac{\partial \rho}{\partial n} \, dsdt \\ &\quad + \int_0^T \int_{\partial\Omega} \left[-\frac{\partial q_1}{\partial n} - q_1 \bar{w} \cdot \vec{n} + q_1 \frac{\partial V_{\text{ext}}}{\partial n} - q_2 \right] \rho \, dsdt. \end{aligned} \quad (3.2)$$

Noting first that (3.2) must hold for all $\rho \in C_0^{\infty}(\Omega \times (0, T))$ (i.e., where $\rho(\vec{x}, T)$, $\rho(\vec{x}, 0)$ vanish on Ω , and $\rho, \frac{\partial \rho}{\partial n}$ vanish on $\partial\Omega$), and observing that $C_0^{\infty}(\Omega \times (0, T))$ is dense on $L^2(\Omega \times (0, T))$, we obtain the adjoint PDE:

$$\mathcal{D}^*(q_1, \vec{w}) := -\partial_t q_1 - \nabla^2 q_1 - \vec{w} \cdot \nabla q_1 + \nabla V_{\text{ext}} \cdot \nabla q_1 = \rho - \hat{\rho} \quad \text{on } \Omega \times (0, T).$$

Removing the restriction that $\rho(\vec{x}, T)$ vanishes on Ω , and arguing similarly, leads to the adjoint boundary condition $q_1(\vec{x}, T) = 0$. From here, we may similarly remove the condition that $\frac{\partial \rho}{\partial n}$ vanishes on $\partial\Omega$ to conclude that $q_1 = 0$ on $\partial\Omega \times (0, T)$. Setting the final integral term in (3.2) to zero then gives the relation between q_1 and q_2 . Putting all the pieces together, and relabelling q_1 as q , we obtain the complete adjoint problem:

$$\begin{aligned} \mathcal{D}^*(q, \vec{w}) &= \rho - \hat{\rho} \quad \text{on } \Omega \times (0, T), \\ q &= 0 \quad \text{at } t = T, \\ q &= 0 \quad \text{on } \partial\Omega \times (0, T). \end{aligned} \quad (3.3)$$

Searching for the stationary point upon differentiation with respect to each component of \vec{w} , using similar working as above, gives:

$$D_{w_i}\mathcal{L}(\bar{\rho}, \bar{w}, q_1, q_2)w_i = \beta \int_0^T \int_{\Omega} \bar{w}_i w_i \, dxdt - \int_0^T \int_{\Omega} \frac{\partial}{\partial x_i} (\bar{\rho} w_i) q_1 \, dxdt.$$

Therefore, using integration by parts,

$$0 = \beta \int_0^T \int_{\Omega} \bar{w}_i w_i \, dxdt + \int_0^T \int_{\Omega} \bar{\rho} \frac{\partial q_1}{\partial x_i} w_i \, dxdt - \int_0^T \int_{\Omega} \frac{\partial}{\partial x_i} (\bar{\rho} q_1 w_i) \, dxdt,$$

whereupon considering the derivatives with respect to the all entries of \vec{w} , and applying Green's formula, leads to the *gradient equation*:

$$\beta \vec{w} + \rho \nabla q = \vec{0}. \quad (3.4)$$

To summarize, the complete first-order optimality system for the problem (2.2) with the Dirichlet boundary condition $\rho = c$ includes the PDE constraint itself (often referred to as the *state equation*), the adjoint problem (3.3), and the gradient equation (3.4).

3.2. Flow control with no-flux type boundary condition. To provide an illustration of how the same working may be applied to problem (2.2) with the no-flux boundary condition (2.4), and $\kappa = 0$, we briefly consider the Lagrangian given by:

$$\mathcal{L}(\rho, \vec{w}, q_1, q_2) = \mathcal{J}(\rho, \vec{w}) - \int_0^T \int_{\Omega} (\mathcal{D}(\rho, \vec{w}) - f) q_1 \, dxdt - \int_0^T \int_{\partial\Omega} \mathcal{N}(\rho, \vec{w}) q_2 \, dsdt.$$

Solving $D_{\rho} \mathcal{L}(\bar{\rho}, \bar{w}, q_1, q_2) \rho = 0$ for all ρ such that $\rho(\vec{x}, 0) = 0$ gives that:

$$\begin{aligned} 0 = & - \int_0^T \int_{\Omega} (\mathcal{D}^*(q_1, \bar{w}) + \hat{\rho} - \bar{\rho}) \rho \, dxdt + \int_{\Omega} q_1(\vec{x}, T) \rho(\vec{x}, T) \, dx \\ & + \int_0^T \int_{\partial\Omega} \left[(q_1 - q_2) \frac{\partial \rho}{\partial n} - \frac{\partial q_1}{\partial n} - (q_1 - q_2) \left(\bar{w} \cdot \bar{n} - \frac{\partial V_{\text{ext}}}{\partial n} \right) \right] \rho \, dsdt. \end{aligned}$$

Applying the same reasoning as above then leads to the adjoint problem:

$$\begin{aligned} \mathcal{D}^*(q, \vec{w}) &= \rho - \hat{\rho} \quad \text{on } \Omega \times (0, T), \\ q &= 0 \quad \text{at } t = T, \\ \frac{\partial q}{\partial n} &= 0 \quad \text{on } \partial\Omega \times (0, T), \end{aligned} \quad (3.5)$$

along with the state equation as in (2.2), and the gradient equation (3.4).

3.3. Source control with Dirichlet boundary condition. We next consider the problem (2.5) with the Dirichlet boundary condition (2.3), and $\kappa = 0$. This leads to the continuous Lagrangian:

$$\mathcal{L}(\rho, w, q_1, q_2) = \mathcal{J}(\rho, w) - \int_0^T \int_{\Omega} (\mathcal{D}_l(\rho, w) - f) q_1 \, dxdt - \int_0^T \int_{\partial\Omega} (\rho - c) q_2 \, dsdt.$$

Solving $D_{\rho} \mathcal{L}(\bar{\rho}, \bar{w}, q_1, q_2) \rho = 0$ for all ρ such that $\rho(\vec{x}, 0) = 0$ gives that:

$$\begin{aligned} 0 = & - \int_0^T \int_{\Omega} (-\partial_t q_1 - \nabla^2 q_1 + \nabla V_{\text{ext}} \cdot \nabla q_1 + \hat{\rho} - \bar{\rho}) \rho \, dxdt \\ & + \int_{\Omega} q(\vec{x}, T) \rho(\vec{x}, T) \, dx + \int_0^T \int_{\partial\Omega} q_1 \frac{\partial \rho}{\partial n} \, dsdt \\ & + \int_0^T \int_{\partial\Omega} \left[-\frac{\partial q_1}{\partial n} + q_1 \frac{\partial V_{\text{ext}}}{\partial n} - q_2 \right] \rho \, dsdt. \end{aligned}$$

Applying the same reasoning as above then leads to the adjoint problem:

$$\begin{aligned} \mathcal{D}_l^*(q) &:= -\partial_t q - \nabla^2 q + \nabla V_{\text{ext}} \cdot \nabla q = \rho - \hat{\rho} && \text{on } \Omega \times (0, T), \\ q &= 0 && \text{at } t = T, \\ q &= 0 && \text{on } \partial\Omega \times (0, T). \end{aligned} \quad (3.6)$$

Searching for the stationary point upon differentiation with respect to w , using similar working as above, gives:

$$D_w \mathcal{L}(\bar{\rho}, \bar{w}, q_1, q_2)w = \beta \int_0^T \int_{\Omega} \bar{w}w \, dxdt + \int_0^T \int_{\Omega} \bar{w}q_1 \, dxdt,$$

leading to the *gradient equation*:

$$\beta w + q = 0. \quad (3.7)$$

To summarize, the complete first-order optimality system for the problem (2.5), with the Dirichlet boundary condition $\rho = c$, includes the PDE constraint itself, the adjoint problem (3.6), and the gradient equation (3.7).

3.4. Source control with no-flux type boundary condition. Applying the same working to problem (2.5) with no-flux boundary condition (2.6), and $\kappa = 0$, the Lagrangian is given by:

$$\mathcal{L}(\rho, \vec{w}, q_1, q_2) = \mathcal{J}(\rho, w) - \int_0^T \int_{\Omega} (\mathcal{D}_l(\rho, w) - f) q_1 \, dxdt - \int_0^T \int_{\partial\Omega} \mathcal{N}_l(\rho) q_2 \, dsdt.$$

Applying the same reasoning as above then leads to the adjoint problem:

$$\begin{aligned} \mathcal{D}_l^*(q) &= \rho - \hat{\rho} && \text{on } \Omega \times (0, T), \\ q &= 0 && \text{at } t = T, \\ \frac{\partial q}{\partial n} &= 0 && \text{on } \partial\Omega \times (0, T), \end{aligned}$$

along with the state equation as in (2.5), and the gradient equation (3.7).

3.5. Optimality system with additional non-local integral term. To conclude this section, we summarize the results of applying the above methodology to the flow control problem (2.2), now with $\kappa \neq 0$. Similarly to the outcomes of Sections 3.1 and 3.2, this results in the following first-order optimality conditions:

$$\left\{ \begin{array}{l} \mathcal{D}(\rho, \vec{w}) - \nabla_r \cdot \mathcal{I}(\rho) = f \quad \text{on } \Omega \times (0, T) \\ \rho = \rho_0(\vec{x}) \quad \text{at } t = 0 \\ \mathcal{D}^*(q, \vec{w}) + \tilde{\mathcal{I}}^*(\rho, q) = \rho - \hat{\rho} \quad \text{on } \Omega \times (0, T) \\ q = 0 \quad \text{at } t = T \\ \beta \vec{w} + \rho \nabla q = \vec{0} \end{array} \right\} \begin{array}{l} \text{state equation} \\ \text{adjoint equation} \\ \text{gradient equation} \end{array}$$

where

$$\tilde{\mathcal{I}}^*(\rho, q) = \kappa \left(\int_{\Omega} \rho(r') \vec{K}(r, r') \, dr' \right) \cdot \nabla_r q(r) + \kappa \int_{\Omega} \left(\rho(r') \vec{K}(r', r) \cdot \nabla_{r'} q(r') \right) \, dr',$$

which is obtained by applying integration by parts and the Divergence Theorem to the term $(\nabla_r \cdot \mathcal{I}(\rho, \vec{w})) q_1$ when deriving the adjoint PDE. Note that this agrees with the representation of the interaction term in [3], where $\kappa \vec{K}(r, r') = P(r, r')(r' - r)$.

For the special case when $\vec{K}(r, r') = \nabla_r V_2(|r - r'|)$, we have that \vec{K} is an odd function in the sense that $\vec{K}(r, r') = -\vec{K}(r', r)$ and

$$\tilde{\mathcal{I}}^*(\rho, q) = \kappa \left(\int_{\Omega} \rho(r') \vec{K}(r, r') \cdot [\nabla_r q(r) - \nabla_{r'} q(r')] \, dr' \right).$$

As in Section 3.1, the boundary condition for the adjoint equation, corresponding to (2.3) in the state equation is

$$q = 0 \quad \text{on } \partial\Omega \times (0, T),$$

regardless of the value of c in (2.3). As in Section 3.2, the boundary condition for the adjoint corresponding to boundary condition (2.4) is

$$\frac{\partial q}{\partial n} = 0 \quad \text{on } \partial\Omega \times (0, T).$$

Note that the boundary conditions for the adjoint equation remain unchanged when adding an interaction term, cf. (3.3) and (3.5), with (3.5) unchanged due to the imposition of the term $\mathcal{I}(\rho) \cdot \vec{n}$ within the boundary condition for ρ .

For the source control problem (2.5), with $\kappa \neq 0$, and boundary condition (2.3) or (2.6), the state and adjoint equations are unchanged, except with $\mathcal{D}(\rho, \vec{w})$, $\mathcal{D}^*(q, \vec{w})$, $\mathcal{N}(\rho, \vec{w})$ replaced by $\mathcal{D}_l(\rho, w)$, $\mathcal{D}_l^*(q, w)$, $\mathcal{N}_l(\rho)$. The gradient equation for this formulation reads $\beta w + q = 0$, as justified in Section 3.3.

4. Numerical Method for Optimization Model. In this section we describe the structure of our algorithm for the PDE-constrained optimization models under consideration. After describing a pseudospectral method for the PDE constraints (the forward problem), and the adjoint equations, we outline our optimization solver, and detail the measures of accuracy that we will employ in our numerical tests.

4.1. Pseudospectral method for the forward problem. As described in Section 2.2, we solve the forward problem using Chebyshev pseudospectral methods, in particular implemented in MATLAB using 2DChebClass [35, 51]. The principal novelties of the method concern the computation of convolution integrals and the implementation of spatial boundary conditions; the boundary conditions in time will be discussed in the following section.

As described in [51], the convolution integrals are computed in real space, in contrast to many implementations in which they are computed via Fourier transforms. The principal advantage of Fourier methods is that they are computationally cheap, requiring only fast Fourier transforms and multiplication of functions. The main disadvantage is that one needs to pad the domain, which both increases computational cost for no accuracy gain and introduces difficulties when applying boundary conditions. Convolution integrals in the spatial method can be implemented by a single matrix–vector multiplication, with the matrix precomputed for all time steps. Use of the physical domain allows efficient implementation of the boundary conditions.

As is standard, after discretization, in this case through the use of (mapped) Chebyshev pseudospectral points, the forward PDE(s) are converted into a system of ODEs. For example, the diffusion equation becomes

$$\frac{d}{dt} \rho = D_2 \rho, \quad + \text{IC and BC}, \tag{4.1}$$

where $\boldsymbol{\rho}$ is a vector of values of the solution at each of the Chebyshev points, and D_2 is the Chebyshev second-order differentiation matrix. In the interior of the domain, this can be solved using standard time-stepping solvers for ODEs. The challenge lies in imposing the correct spatial boundary conditions. One standard approach is to modify the matrix on the right hand side of (4.1) so that the boundary conditions are automatically satisfied. This is known as ‘boundary-bordering’ [13]. For simple boundary conditions, such as homogenous Dirichlet or (local) Neumann, such an approach is relatively straightforward. For example, for homogeneous Dirichlet conditions, assuming that the initial conditions satisfy the boundary conditions, it is sufficient to set the first and last rows and columns of D_2 to zero. For homogeneous Neumann, there is a similar approach (see [65]), which becomes more involved with more complex right-hand sides of the PDE. Another approach is to restrict the computation to interpolants (solutions) which satisfy the boundary conditions; we do not discuss this here as it is highly non-trivial for the non-linear, non-local problems that we are interested in.

Here we take a more general approach. The imposition of spatial boundary conditions can be seen as extending the discretized system of ODEs to a system of differential–algebraic equations, where the discretized PDE is solved on the interior of the domain, and the boundary conditions correspond to algebraic equations. There are various numerical methods for solving such differential–algebraic equations, e.g., [60]. The main advantage here is that the numerical method does not have to be explicitly adapted when one changes the boundary conditions; one simply has to specify different algebraic constraints that correspond to the boundary conditions. In fact, the 2DChebClass code automatically identifies the boundary of various geometries, allowing a simple implementation of this approach.

4.2. Pseudospectral method for the adjoint equation. For the optimization problem, we have a pair of coupled PDEs: the forward PDE with an initial time condition, and the adjoint equation with a final time condition. Hence, one cannot use a standard time-stepping scheme, as there are Laplacians of opposite signs in the forward and adjoint equations; the adjoint equation is unstable ‘forward in time’.

One approach is to apply a backward Euler method for the time derivative in the state equation, with the adjoint operator applied to the adjoint equation, whereupon a huge-scale coupled system of equations is obtained from matrices arising at each time-step. These may be tackled using a preconditioned iterative method, following the methodology in [52, 53, 61], for instance. As above, as well as boundary conditions in time, there are also boundary conditions in space.

In contrast, in order to utilize our efficient and accurate forward solver, we reverse time in the adjoint problem, resulting in a set of well-posed equations with initial conditions. However, the forward and adjoint equations are coupled non-locally in time; the adjoint equation requires the value of the state variable at later times, so the two equations cannot be solved simultaneously. This difficulty is addressed using the fixed point algorithm presented in the next section.

4.3. Optimization solver. The remaining challenges are to (i) determine the time discretization for the optimality system; (ii) choose a suitable optimization scheme. For (i), we again choose a Chebyshev pseudospectral scheme (1D in time), which, assuming that the solutions are smooth in time, leads to exponentially accurate interpolation. As mentioned in Section 4.1 the system of ODEs, and the differential–algebraic equations resulting from applying the pseudospectral method, can be solved using a standard DAE solver. In this paper, the MATLAB inbuilt ODE solver `ode15s`

is used. For (ii), we note that the choice of optimization solver depends strongly on the nature of the solution, and the amount of information available. For ease of implementation, and to remove the need to, e.g., analytically compute the Jacobian, we use a fixed point method. Though our approach is highly modular and it is straightforward to replace this solver with any other optimization routine, we adapt a fixed point or sweeping method [3, 16] to solve the system of equations iteratively.

In the following, we denote the discretized versions of the variables ρ , q , and \vec{w} by P , Q , and W , respectively. Each of these matrices is of the form $A = [\mathbf{a}_0, \mathbf{a}_1, \dots, \mathbf{a}_n]$, where the vectors \mathbf{a}_k represent the solutions at the discretized times $k \in \{0, 1, \dots, n\}$, where n is the number of time steps. In particular, the first column of P , denoted by $\boldsymbol{\rho}_0$, corresponds to the initial condition $\rho(\vec{x}, 0)$. If the spatial domain is one-dimensional, P , Q , and W are of size $N \times (n + 1)$, where N is the number of spatial points. In the two-dimensional case, P and Q are of size $(N_1 N_2) \times (n + 1)$, where N_j is the number of spatial points in the direction of x_j . The discretized control W for linear (source) control problems is also $(N_1 N_2) \times (n + 1)$ dimensional, while it is $(2N_1 N_2) \times (n + 1)$ dimensional for non-linear (flow) control problems.

The optimization algorithm is initialized with a guess for the control, $W^{(0)}$. Then, in each iteration, denoted by i , the following steps are computed:

1. Starting with a guess for the control $W^{(i)}$ as input variable, the corresponding state $P^{(i)}$ is found by solving the forward equation.
2. The adjoint, $Q^{(i)}$, is obtained as the solution of the (reversed in time) adjoint equation, using $W^{(i)}$ and $P^{(i)}$ as inputs. Since $P^{(i)}$ contains the solution for all discretized times $k \in \{0, 1, \dots, n\}$, pseudospectral interpolation circumvents issues resulting from the non-local coupling in time, mentioned in Section 4.2.
3. The obtained $P^{(i)}$ and $Q^{(i)}$ are used to solve the gradient equation for the updated control, $W_g^{(i)}$.
4. The convergence of the optimization scheme is measured by computing the error, \mathcal{E} , between $W^{(i)}$ and $W_g^{(i)}$; see Section 4.4. If \mathcal{E} is smaller than a set tolerance, the algorithm terminates, otherwise we proceed to Step 5.
5. We update $W^{(i+1)}$ as a linear combination of the current guess $W^{(i)}$, and the value obtained in step 3, $W_g^{(i)}$, employing a mixing rate $\lambda \in [0, 1]$:

$$W^{(i+1)} = (1 - \lambda)W^{(i)} + \lambda W_g^{(i)}.$$

The update scheme in Step 5, with mixing rate λ , is known to stabilize such fixed point methods, see e.g., [59]. Typical values of λ , which provide stable convergence in the cases we study here, lie between 0.1 and 0.001; we choose $\lambda = 0.01$, unless otherwise stated. As mentioned previously, this mixing scheme is similar to the updating scheme presented in [16]. Note that, while the solutions $P^{(i)}$ and $Q^{(i)}$ change in each iteration, the initial condition $\boldsymbol{\rho}_0$ and final time condition \mathbf{q}_n remain unchanged throughout the process; the updates are induced by changing $W^{(i)}$.

4.4. Measures of accuracy. All errors in Sections 4.4 and 5 are calculated as a measure of the difference between a variable of interest, y , and a reference value y_R , e.g., a previous value of $W^{(i)}$, or an exact solution to a test problem. The error measure \mathcal{E} is composed of an L^2 error in space and an L^∞ error in time. We define

absolute and relative L^2 spatial errors

$$\mathcal{E}_{Abs}(t) = \|y(\vec{x}, t) - y_R(\vec{x}, t)\|_{L^2(\Omega)},$$

and

$$\mathcal{E}_{Rel}(t) = \frac{\|y(\vec{x}, t) - y_R(\vec{x}, t)\|_{L^2(\Omega)}}{\|y_R(\vec{x}, t)\|_{L^2(\Omega)} + 10^{-10}},$$

where the small additional term on the denominator prevents division by zero, which are used in the full error measure:

$$\mathcal{E} = \max_{t \in [0, T]} [\min(\mathcal{E}_{Rel}(t), \mathcal{E}_{Abs}(t))].$$

The minimum between absolute and relative spatial error is taken to avoid choosing an erroneously large relative error, caused by division of one numerically very small term by another.

As a benchmark, we compared the fixed point scheme to MATLAB's inbuilt `fsolve` function. It uses the trust-region-dogleg algorithm, see [56], to solve the optimality system of interest. While it is very robust, it is also much slower than the fixed point method, which works reliably for the types of problems considered in this paper. A comparison is given in the Supplementary Material, along with numerical results for specific test problems with analytic solutions (with $\kappa = 0$), and further tests to validate our method.

5. Numerical Experiments. The optimal control problems (2.2) and (2.5) require inputs in terms of the desired state $\hat{\rho}$, the PDE source term f , and the external potential V_{ext} , alongside initial and final time conditions for ρ and q , respectively. These are stated for the individual examples below. We also require an interaction kernel, which here we fix as

$$\vec{K}(\vec{r}, \vec{r}') = \nabla V_2(\vec{r} - \vec{r}'), \quad V_2(\vec{x}) = e^{-\|\vec{x}\|^2}.$$

Interest lies in how the solution to the optimization problems changes upon varying the interaction strength, κ . Here we consider three representative values: $\kappa = 0$ (no interaction), $\kappa = -1$ (attraction), and $\kappa = 1$ (repulsion).

As a baseline, we solve the forward PDE using $\vec{w} = \vec{0}$. We evaluate the associated cost functional \mathcal{J} , the value of which is denoted by \mathcal{J}_{uc} . We then expect that applying the optimization method lowers the value of the cost functional, which we then aim to minimize by optimizing \vec{w} , resulting in a cost \mathcal{J}_c . This cost depends on the value of the regularization parameter β and it is expected that the optimal amount of control applied will increase with decreasing β . For the initial guess for the control in the optimization algorithm, we take $\vec{w} = \vec{0}$, corresponding to the reference system.

In the following examples, the domain considered is $\Omega \times (0, T) = (-1, 1)^d \times (0, 1)$. The number of spatial points is $N = 30$ in one-dimensional examples, $N_1 = N_2 = 30$ in two-dimensional examples, and the number of time points is $n = 20$, unless stated otherwise. The tolerances in the ODE and optimization solvers are set to 10^{-8} and 10^{-4} , respectively. As noted above, the mixing parameter λ is 0.01, unless stated otherwise.

5.1. Non-linear (flow) control problems in 1D. We first present examples involving the flow control problem (2.2) with additional non-local integral term, equipped with 'no-flux type' boundary conditions (2.4) and Dirichlet boundary conditions (2.3).

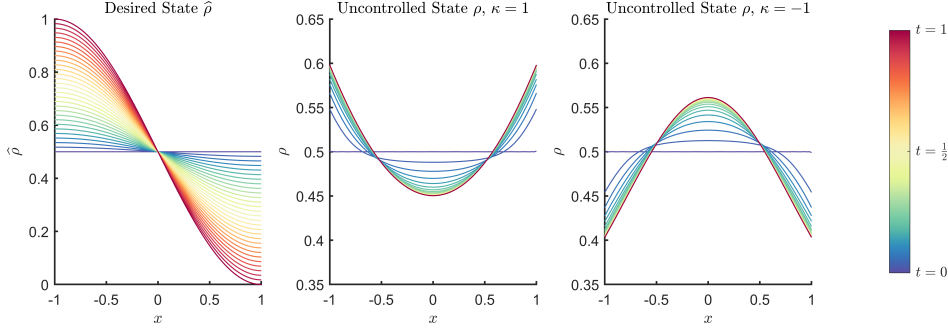


FIG. 5.1. *Example 1: Desired state $\hat{\rho}$ and uncontrolled state ρ for $\kappa = 1$ and $\kappa = -1$. Colours denote different times.*

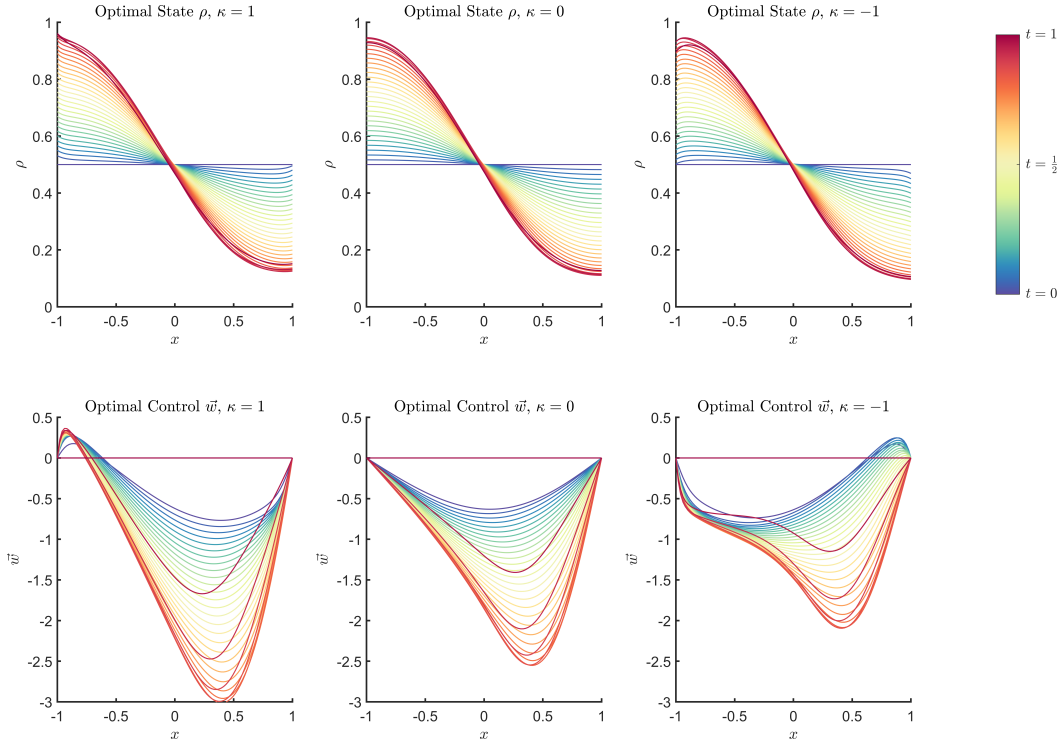


FIG. 5.2. *Example 1: Optimal state ρ and corresponding optimal control \bar{w} for $\kappa = 1, 0, -1$, $\beta = 10^{-3}$.*

5.1.1. No-flux type boundary conditions, Example 1. The chosen inputs for this example are:

$$\hat{\rho} = \frac{1-t}{2} + \frac{t}{2} \left(\sin \left(\frac{\pi(x-2)}{2} \right) + 1 \right), \quad \rho_0 = \frac{1}{2}, \quad f = 0, \quad V_{\text{ext}} = 0.$$

In Table 5.1, the value of the cost functional for the initial configuration (\mathcal{J}_{uc}), where $\bar{w} = 0$, is compared with the optimized case (\mathcal{J}_c) for different values of β and for each of the interaction strengths. As expected, in all cases $\mathcal{J}_c \leq \mathcal{J}_{uc}$ and the lowest values of \mathcal{J}_c occur for the smallest β values. For large values of β , applying control is

		$\beta = 10^{-3}$	$\beta = 10^{-1}$	$\beta = 10^1$	$\beta = 10^3$
$\kappa = -1$	\mathcal{J}_{uc}	0.0438	0.0438	0.0438	0.0438
	\mathcal{J}_c	0.0011	0.0267	0.0435	0.0438
	Iter	670	650	449	1
$\kappa = 0$	\mathcal{J}_{uc}	0.0417	0.0417	0.0417	0.0417
	\mathcal{J}_c	0.0014	0.0283	0.0415	0.0417
	Iter	665	656	434	1
$\kappa = 1$	\mathcal{J}_{uc}	0.0434	0.0434	0.0434	0.0434
	\mathcal{J}_c	0.0020	0.0322	0.0432	0.0434
	Iter	654	682	422	1

TABLE 5.1

*Example 1: Cost \mathcal{J}_{uc} of applying no control (i.e., $\vec{w} = \vec{0}$), optimal control cost \mathcal{J}_c , and number of iterations (PDE solves) **Iter** required, for a range of values of the interaction strength κ and regularization parameter β .*

heavily penalized and the optimal control approaches zero, which coincides with the uncontrolled case. This is reflected in the number of iterations **Iter**, which is small when β is large (and $\vec{w} = \vec{0}$ is a good initial guess), and vice versa. We note that we show results up to the very large value $\beta = 10^3$, purely to demonstrate that the number of iterations required is very low due to the model allowing the imposition of almost no control.

The desired state $\hat{\rho}$ and uncontrolled state ρ , for $\kappa = 1$ and $\kappa = -1$, are shown in Figure 5.1. Note that they are independent of β . The uncontrolled ρ depends strongly on the interaction strength κ , accumulating mass in the centre of the domain for attractive interactions and at the boundary for repulsive interactions, suggesting that different optimal controls will be required. The optimal states ρ for $\kappa = 1, 0, -1$ and corresponding optimal controls, with $\beta = 10^{-3}$, are shown in Figure 5.2. For this (relatively small) value of β , the optimal state ρ is very similar to $\hat{\rho}$, regardless of the choice of interaction. However, the corresponding control plots reveal the effects of interactions on the optimal controls. In general, the control is largely applied on the right half of the spatial domain, to carry mass towards the target state on the left. The main effects of κ can be seen near the boundaries. When $\kappa = 1$ (repulsive), the control moves some of the particle mass away from the boundary at $x = -1$ to correct for the uncontrolled accumulation, as illustrated in Figure 5.1. Analogously, in the attractive case, the control carries some mass to the boundary at $x = 1$, which counters the natural depletion.

5.1.2. No-flux type boundary conditions, Example 2. The chosen inputs for our next example are:

$$\hat{\rho} = \frac{1-t}{2} (\cos(\pi x) + 1) + \frac{t}{2} (-\cos(2\pi x) + 1), \quad \rho_0 = \frac{1}{2} \cos(\pi x) + \frac{1}{2}, \quad f = 0, \quad V_{\text{ext}} = 0,$$

and the corresponding results are shown in Table 5.2. We observe the same trends with respect to β and the number of iterations as for Example 1. For all three choices of κ , the control is focussed on transporting the mass from the middle of the domain onto two piles centred at $x = -0.5$ and $x = 0.5$. We show the results for $\kappa = 1$ and $\beta = 10^{-3}$ in Figure 5.3. We note in particular the complexity of the optimal control. This problem is numerically more challenging than the previous one, and we choose $N = 40$ and $n = 30$ (instead of $N = 30$ and $n = 20$). We believe this is a consequence

		$\beta = 10^{-3}$	$\beta = 10^{-1}$	$\beta = 10^1$	$\beta = 10^3$
$\kappa = -1$	\mathcal{J}_{uc}	0.0536	0.0536	0.0536	0.0536
	\mathcal{J}_c	0.0096	0.0492	0.0535	0.0536
	Iter	715	767	367	1
$\kappa = 0$	\mathcal{J}_{uc}	0.0669	0.0669	0.0669	0.0669
	\mathcal{J}_c	0.0109	0.0603	0.0668	0.0669
	Iter	714	770	390	1
$\kappa = 1$	\mathcal{J}_{uc}	0.0839	0.0839	0.0839	0.0839
	\mathcal{J}_c	0.0125	0.0748	0.0838	0.0839
	Iter	713	773	403	1

TABLE 5.2

Example 2: Cost when $\vec{w} = \vec{0}$, optimal control cost, and iterations required, for a range of κ , β .

		$\beta = 10^{-3}$	$\beta = 10^{-1}$	$\beta = 10^1$	$\beta = 10^3$
$\kappa = -1$	\mathcal{J}_{uc}	0.1417	0.1417	0.1417	0.1417
	\mathcal{J}_c	0.0354	0.1326	0.1416	0.1417
	Iter	925	811	439	1
$\kappa = 0$	\mathcal{J}_{uc}	0.1545	0.1545	0.1545	0.1545
	\mathcal{J}_c	0.0380	0.1455	0.1544	0.1545
	Iter	940	825	440	1
$\kappa = 1$	\mathcal{J}_{uc}	0.1661	0.1661	0.1661	0.1661
	\mathcal{J}_c	0.0409	0.1574	0.1660	0.1661
	Iter	955	835	439	1

TABLE 5.3

Example 3: Cost when $\vec{w} = \vec{0}$, optimal control cost, and iterations required, for a range of κ , β .

of the steep optimal control and state, which requires a more accurate numerical resolution. We next study the effects of the boundary condition on the dynamics and control; Figure 5.3 also shows the results for the corresponding Dirichlet case, described below.

5.1.3. Dirichlet boundary conditions, Example 3. Here we use the same inputs as in Example 2, but replace the no-flux boundary conditions with Dirichlet conditions. Table 5.3 again shows the results for a range of β values and different interaction strengths; the results for $\kappa = 1$ and $\beta = 10^{-3}$ are shown in Figure 5.3. The observations are in line with those in Example 1 and 2. However, both the optimal state ρ and the optimal control are qualitatively different when considering Dirichlet boundary conditions rather than no-flux conditions, requiring more control to be applied in the Dirichlet case than in the no-flux example. We find the Dirichlet case to also be challenging numerically, requiring us to increase the number of points to $N = 40$ and $n = 30$ (rather than $N = 30$ and $n = 20$).

5.2. Linear (source) control problems in 1D. Here we show examples of solving the source control problem (2.5), with no-flux type boundary conditions (2.6) and Dirichlet boundary conditions (2.3).

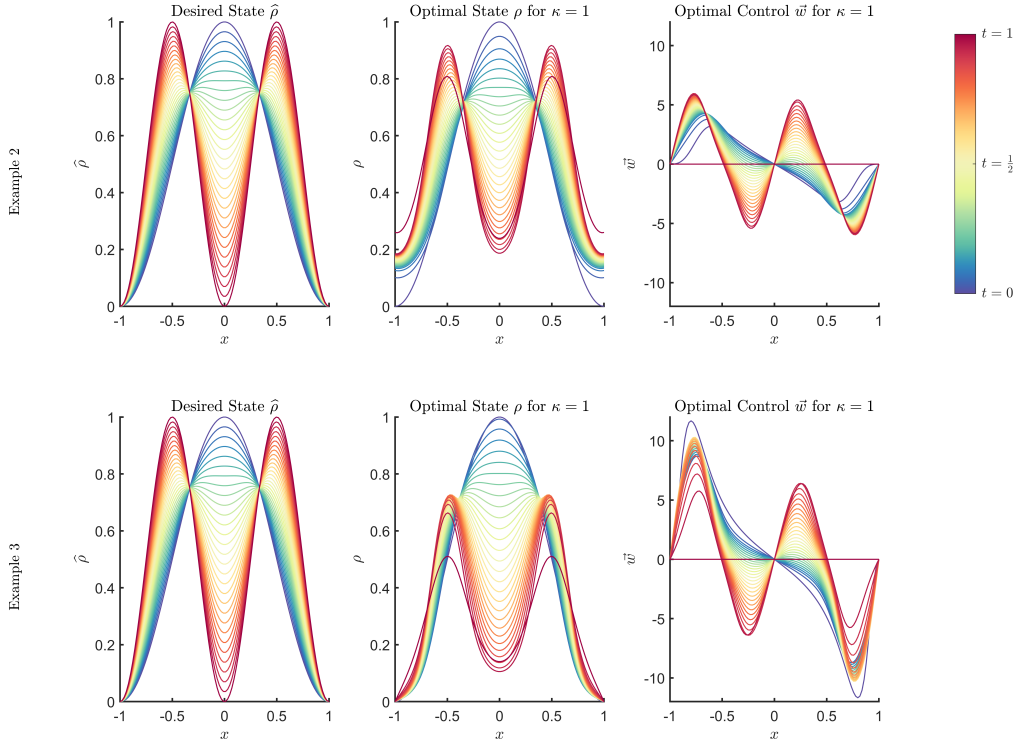


FIG. 5.3. *Example 2/Example 3: Desired state $\hat{\rho}$, optimal state ρ and corresponding optimal control with \bar{w} , $\beta = 10^{-3}$ and $\kappa = 1$. Example 2 has no-flux boundary conditions, whereas Dirichlet boundary conditions are applied in Example 3.*

5.2.1. Dirichlet boundary conditions, Example 4. The inputs here are:

$$\hat{\rho} = \frac{1-t}{2} (\cos(\pi x) + 1) + \frac{t}{2} (-\cos(\pi x) + 1), \quad \rho_0 = \frac{1}{2} \cos(\pi y) + \frac{1}{2}, \quad f = 0,$$

$$V_{\text{ext}} = -\frac{1}{2} ((x+0.3)^2 - 0.2) ((x-0.4)^2 - 0.3).$$

We show results for this problem in Table 5.4; they are qualitatively similar to the previous examples. Note that here $\lambda = 0.005$, since V_{ext} causes the fixed point optimization computations to be more challenging.

5.2.2. No-flux type boundary conditions, Example 5. The inputs are:

$$\hat{\rho} = \frac{1-t}{2} + \frac{t}{2} (-\cos(\pi x) + 1), \quad \rho_0 = \frac{1}{2}, \quad f = 0, \quad V_{\text{ext}} = 0.$$

The corresponding results are shown in Table 5.5. The mixing parameter λ is set to 0.001 and the number of points is increased to $N = 40$ and $n = 30$, to guarantee stable convergence of the method.

5.3. Non-linear (flow) control problems in 2D. In this section, we demonstrate the modular and flexible nature of our approach by applying it to problems in two spatial dimensions. The main difference is that the PDE discretization requires an increased number of points from N to $N_1 N_2$, where N_j are typically of order N , resulting in increased computational cost. This is a key motivation for the development

		$\beta = 10^{-3}$	$\beta = 10^{-1}$	$\beta = 10^1$	$\beta = 10^3$
$\kappa = -1$	\mathcal{J}_{uc}	0.1394	0.1394	0.1394	0.1394
	\mathcal{J}_c	0.0183	0.0862	0.1384	0.1394
	Iter	1575	1486	1026	117
$\kappa = 0$	\mathcal{J}_{uc}	0.1526	0.1526	0.1526	0.1526
	\mathcal{J}_c	0.0183	0.0983	0.1516	0.1526
	Iter	1582	1474	1023	113
$\kappa = 1$	\mathcal{J}_{uc}	0.1645	0.1645	0.1645	0.1645
	\mathcal{J}_c	0.0189	0.1103	0.1635	0.1645
	Iter	1589	1465	1022	112

TABLE 5.4

Example 4: Cost when $w = 0$, optimal control cost, and iterations required, for a range of κ , β .

		$\beta = 10^{-3}$	$\beta = 10^{-1}$	$\beta = 10^1$	$\beta = 10^3$
$\kappa = -1$	\mathcal{J}_{uc}	0.0606	0.0606	0.0606	0.0606
	\mathcal{J}_c	0.0060	0.0541	0.0605	0.0606
	Iter	7024	7731	3961	1
$\kappa = 0$	\mathcal{J}_{uc}	0.0417	0.0417	0.0417	0.0417
	\mathcal{J}_c	0.0045	0.0383	0.0416	0.0417
	Iter	7003	7618	3642	1
$\kappa = 1$	\mathcal{J}_{uc}	0.0286	0.0286	0.0286	0.0286
	\mathcal{J}_c	0.0036	0.0261	0.0285	0.0286
	Iter	7052	7490	3474	1

TABLE 5.5

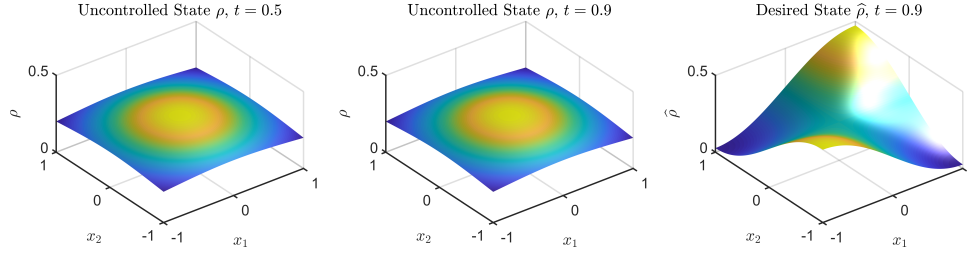
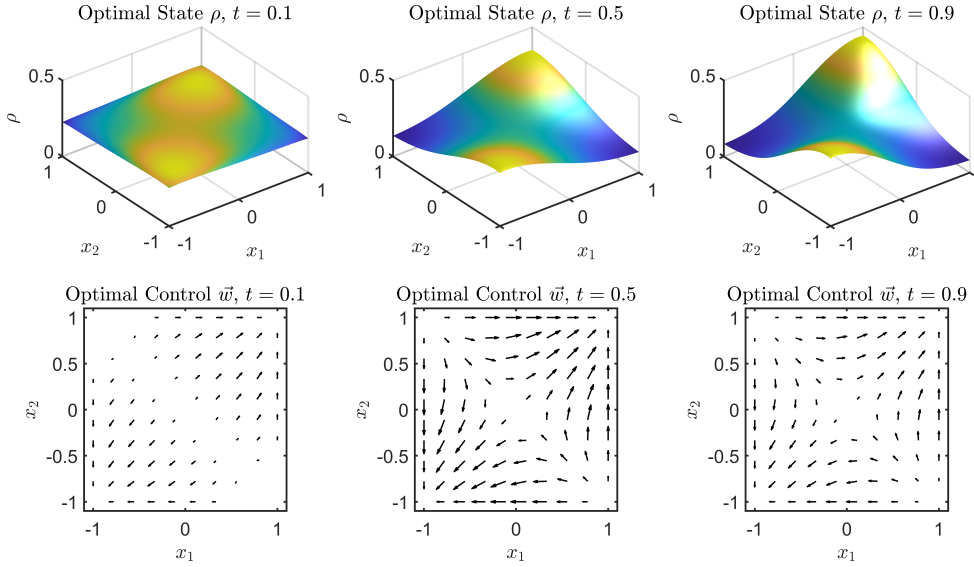
Example 5: Cost when $w = 0$, optimal control cost, and iterations required, for a range of κ , β .

of fast optimization solvers, such as the fixed point method introduced in Section 4.3. Note that here the non-linear control becomes a true (2D) vector field, rather than a scalar field as it is in the 1D case.

5.3.1. No-flux type boundary conditions, 2D Example 1. For this example we have the following set up:

$$\hat{\rho} = \frac{1-t}{4} + \frac{t}{4} \left(\sin \left(\frac{\pi(x_1-2)}{2} \right) \sin \left(\frac{\pi(x_2-2)}{2} \right) + 1 \right), \quad \rho_0 = \frac{1}{4}, \quad f = 0, \quad V_{\text{ext}} = 0,$$

where $\vec{x} = [x_1, x_2]^\top$. This example is a two-dimensional analogue of Example 1 in Section 5.1. The results for this example are displayed in Table 5.6. Figure 5.4 shows the uncontrolled state and the desired state with $\kappa = 1$ and $\beta = 10^{-3}$, with the optimal state and control shown in Figure 5.5. We see that due to the attractive nature of the interactions, as in Example 1 in Section 5.1, the uncontrolled state forms a cluster in the centre of the domain. The dynamics displayed in Figure 5.5 illustrate that the optimal state is close to $\hat{\rho}$ at all times, due to the small value of β . The optimal control carries particles in the direction of the two corners $(-1, -1)$, $(1, 1)$, as prescribed by the desired state. It acts particularly strongly on the emerging slopes of the two piles, since steep mass accumulation is hard to achieve under the influence of diffusion and interaction forces.

FIG. 5.4. 2D Example 1: Uncontrolled ρ and desired state $\hat{\rho}$, with $\beta = 10^{-3}$ and $\kappa = -1$.FIG. 5.5. 2D Example 1: Controlled ρ and optimal control \vec{w} , with $\beta = 10^{-3}$ and $\kappa = -1$.

5.3.2. No-flux type boundary conditions, 2D Example 2.

Here, we have $\hat{\rho} = \frac{1-t}{4} + \frac{t}{Z} e^{-3((x_1+0.2)^2+(x_2+0.2)^2)}$, $\rho_0 = \frac{1}{4}$, $f = 0$,

$$V_{\text{ext}} = ((x_1 + 0.3)^2 - 1) ((x_1 - 0.4)^2 - 0.5) ((x_2 + 0.3)^2 - 1) ((x_2 - 0.4)^2 - 0.5),$$

with $Z \approx 0.9921$ a normalization constant. The numerical results for this example are displayed in Table 5.7. In Figures 5.6 and 5.7 the results are illustrated for $\beta = 10^{-3}$ and $\kappa = -1$. Figure 5.6 demonstrates the effect of V_{ext} on the state. The particle mass accumulates in regions with potential wells and the areas where the potential is steep are avoided. In Figure 5.7 it can be observed very clearly that the control is driving the particle distribution to the desired state. It is noticeable that the control does not act uniformly around the peak of the desired state, but also acts strongly in the area between the location of the desired peak and the point $(-1, 1)$. This is due to the external potential being steep in this area and more control is needed to reach the desired state than in other parts of the domain.

6. Concluding Remarks. We have derived an accurate and efficient algorithmic strategy for solving the first-order optimality conditions arising from PDE-constrained optimization problems, along with additional integral terms, describing

		$\beta = 10^{-3}$	$\beta = 10^{-1}$	$\beta = 10^1$	$\beta = 10^3$
$\kappa = -1$	\mathcal{J}_{uc}	0.0113	0.0113	0.0113	0.0113
	\mathcal{J}_c	0.0013	0.0104	0.0113	0.0113
	Iter	676	700	290	1
$\kappa = 0$	\mathcal{J}_{uc}	0.0104	0.0104	0.0104	0.0104
	\mathcal{J}_c	0.0013	0.0096	0.0104	0.0104
	Iter	676	688	289	1
$\kappa = 1$	\mathcal{J}_{uc}	0.0111	0.0111	0.0111	0.0111
	\mathcal{J}_c	0.0016	0.0102	0.0111	0.0111
	Iter	679	683	290	1

TABLE 5.6

2D Ex. 1: Cost when $\bar{w} = \bar{0}$, optimal control cost, and iterations required, for a range of κ, β .

		$\beta = 10^{-3}$	$\beta = 10^{-1}$	$\beta = 10^1$	$\beta = 10^3$
$\kappa = -1$	\mathcal{J}_{uc}	0.0400	0.0400	0.0400	0.0400
	\mathcal{J}_c	0.0046	0.0370	0.0400	0.0400
	Iter	717	778	347	1
$\kappa = 0$	\mathcal{J}_{uc}	0.0478	0.0478	0.0478	0.0478
	\mathcal{J}_c	0.0064	0.0450	0.0478	0.0478
	Iter	718	784	343	1
$\kappa = 1$	\mathcal{J}_{uc}	0.0556	0.0556	0.0556	0.0556
	\mathcal{J}_c	0.0085	0.0530	0.0556	0.0556
	Iter	720	787	339	1

TABLE 5.7

2D Ex. 2: Cost when $\bar{w} = \bar{0}$, optimal control cost, and iterations required, for a range of κ, β .

multiscale particle dynamics problems. Our approach, linked to the DDFT approach applied to (non-optimized) systems in statistical mechanics, applies a pseudospectral method in both time and space, and utilizes a fixed point scheme within the optimization solver. This novel methodology is more general in scope than existing numerical implementations for similar problems, and exhibits the substantial computational benefits of applying such methods for non-local, non-linear systems of PDEs. Numerical tests indicate the potency of our approach for a range of examples, boundary conditions, and problem parameters (see also the Supplementary Material). There are many possible extensions to our approach: for instance, one may apply our methodology to problems where the misfit between state and desired state is measured at some final time only, models with different cost functionals, and boundary control problems. Furthermore, methods of this type may be tailored to specific particle dynamics applications, in fields such as opinion dynamics, flocking, swarming, and optimal control problems in robotics, and a number of such applications will be tackled in future work.

Acknowledgements. MA and JCR are supported by The Maxwell Institute Graduate School in Analysis and its Applications, a Centre for Doctoral Training funded by the UK Engineering and Physical Sciences Research Council (EPSRC grant EP/L016508/01), the Scottish Funding Council, Heriot-Watt University, and The University of Edinburgh. BDG gratefully acknowledges support from the EPSRC grant EP/L025159/1. JWP gratefully acknowledges support from the EPSRC

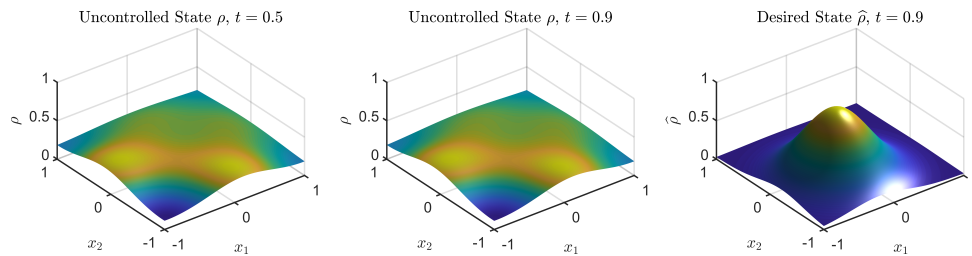


FIG. 5.6. 2D Example 2: Uncontrolled ρ and desired state $\hat{\rho}$, with $\beta = 10^{-3}$ and $\kappa = -1$.

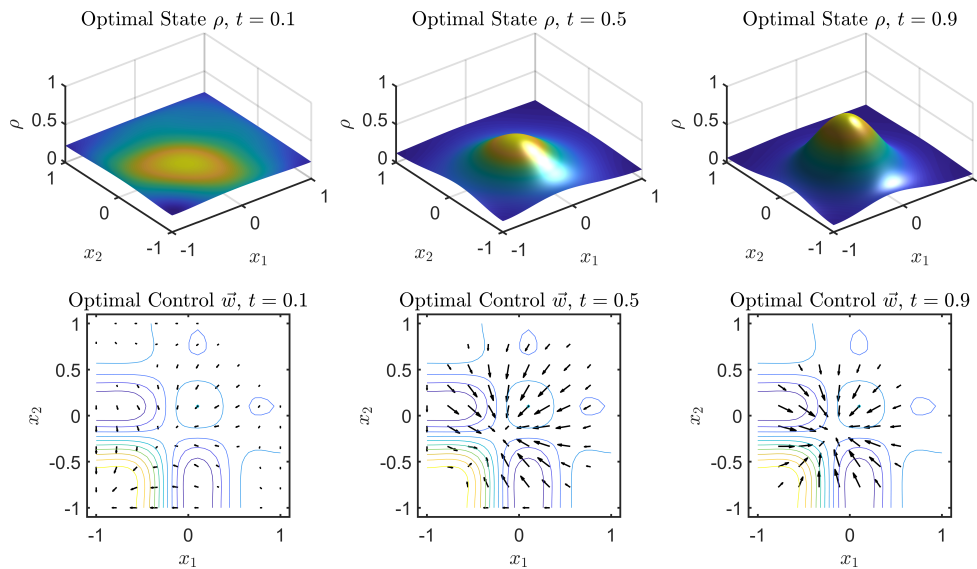


FIG. 5.7. 2D Example 2: Optimal state ρ and optimal control \vec{w} , with $\beta = 10^{-3}$ and $\kappa = -1$. A contour plot of the external potential V_{ext} is superimposed on the control plots for reference.

Fellowship EP/M018857/2, the EPSRC grant EP/S027785/1, and a Fellowship from The Alan Turing Institute.

REFERENCES

- [1] M Aduamoah, B. D. Goddard, J. W. Pearson, and J. Roden. 2DChebClassPDECO [Software]. <https://bitbucket.org/bdgoddard/2dchebclasspdecopublic/>, 2020.
- [2] G. Albi, M. Bongini, E. Cristiani, and D. Kalise. Invisible control of self-organizing agents leaving unknown environments. *SIAM J. Appl. Math.*, 76(4):1683–1710, 2016.
- [3] G. Albi, Y.-P. Choi, M. Fornasier, and D. Kalise. Mean field control hierarchy. *Appl. Math. Opt.*, 76:93–135, 2017.
- [4] G. Albi, M. Herty, and L. Pareschi. Kinetic description of optimal control problems and applications to opinion consensus. *Commun. Math. Sci.*, 13(6):1407–1429, 2014.
- [5] G. Albi and D. Kalise. (Sub)Optimal feedback control of mean field multi-population dynamics. *IFAC-PapersOnLine*, 51(3):86–91, 2018.
- [6] G. Albi and L. Pareschi. Selective model-predictive control for flocking systems. *Commun. Appl. Ind. Math.*, 9(2):4–21, 2018.
- [7] G. Albi, L. Pareschi, and M. Zanella. Boltzmann-type control of opinion consensus through leaders. *Philos. Trans. Roy. Soc. A*, 372(2028):20140138, 2014.
- [8] W. Alt, M. Chaplain, M. Griebel, and J. Lenz, editors. *Polymer and Cell Dynamics: Multiscale Modelling and Numerical Simulations*. Birkhäuser, 2012.

- [9] A. J. Archer, B. Chacko, and R. Evans. The standard mean-field treatment of inter-particle attraction in classical DFT is better than one might expect. *J. Chem. Phys.*, 147(3):034501, 2017.
- [10] H. Aubin, J. W. Nichol, C. B. Hutson, H. Bae, A. L. Sieminski, D. M. Crokek, P. Akhyari, and A. Khademhosseini. Directed 3D cell alignment and elongation in microengineered hydrogels. *Biomaterials*, 31(27):6941–6951, 2010.
- [11] J. Binney and S. Tremaine. *Galactic Dynamics*. Princeton University Press, 2011.
- [12] M. Bongini and G. Buttazo. Optimal control problems in transport dynamics. *Math. Models Methods Appl. Sci.*, 27(3):427–451, 2017.
- [13] J. P. Boyd. *Chebyshev and Fourier Spectral Methods*. Courier Corporation, 2001.
- [14] L. M. Briceño Aras, D. Kalise, and F. J. Silva. Proximal methods for stationary mean field games with local couplings. *SIAM J. Control Opt.*, 56(2):801–836, 2018.
- [15] M. Bruna and S. J. Chapman. Excluded-volume effects in the diffusion of hard spheres. *Phys. Rev. E*, 85(1):011103, 2012.
- [16] M. Burger, M. Di Francesco, P. A. Markowich, and M.-T. Wolfram. Mean field games with nonlinear mobilities in pedestrian dynamics. *Discrete Cont. Dyn.-B*, 19(5):1311–1333, 2014.
- [17] M. Burger, R. Pinnau, A. Roth, C. Totzeck, and O. Tse. Controlling a self-organizing system of individuals guided by a few external agents – Particle description and mean-field limit. *arXiv e-prints*, arXiv:1610.01325, 2016.
- [18] M. Burger, R. Pinnau, C. Totzeck, and O. Tse. Mean-field optimal control and optimality conditions in the space of probability measures. *arXiv e-prints*, arXiv:1902.05339, 2019.
- [19] M. Burger, R. Pinnau, C. Totzeck, O. Tse, and A. Roth. Instantaneous control of interacting particle systems in the mean-field limit. *J. Comput. Phys.*, 405:109181, 2020.
- [20] J. A. Carrillo, Y.-P. Choi, C. Totzeck, and O. Tse. An analytical framework for consensus-based global optimization method. *Math. Models Methods Appl. Sci.*, 28(6):1037–1066, 2018.
- [21] J. A. Carrillo, E. A. Pimentel, and V. K. Voskanyan. On a mean field optimal control problem. *Nonlinear Anal.*, 199:112039, 2020.
- [22] G. K.-L. Chan and R. Finken. Time-dependent density functional theory of classical fluids. *Phys. Rev. Lett.*, 94(18):183001, 2005.
- [23] C. Z. Cheng and G. Knorr. The integration of the Vlasov equation in configuration space. *J. Comput. Phys.*, 22(3):330–351, 1976.
- [24] S. S. Collis and M. Heinkenschloss. Analysis of the streamline upwind/Petrov Galerkin method applied to the solution of optimal control problems. Technical Report TR02–01, Department of Computational and Applied Mathematics, Rice University, 2002.
- [25] E. Cristiani and D. Peri. Robust design optimization for egressing pedestrians in unknown environments. *Appl. Math. Model.*, 72:553–568, 2019.
- [26] E. Cristiani, B. Piccoli, and A. Tosin. *Multiscale Modeling of Pedestrian Dynamics*. Springer, 2014.
- [27] F. Cucker and S. Smale. Emergent behavior in flocks. *IEEE Trans. Automat. Control*, 52(5):852–862, 2007.
- [28] F. Cucker and S. Smale. On the mathematics of emergence. *Jpn. J. Math.*, 2:197–227, 2007.
- [29] R. Evans. The nature of the liquid-vapour interface and other topics in the statistical mechanics of non-uniform, classical fluids. *Adv. Phys.*, 28(2):143, 1979.
- [30] R. Evans. Density functionals in the theory of nonuniform fluids. In D. Henderson, editor, *Fundamentals of Inhomogeneous Fluids*, pages 85–175. Marcel Dekker, 1992.
- [31] M. Fornasier. Learning and sparse control of multiagent systems. In *7th European Congress of Mathematics*, 2016.
- [32] M. Fornasier, S. Lisini, C. Orrieri, and G. Savaré. Mean-field optimal control as Gamma-limit of finite agent controls. *European J. Appl. Math.*, 30(6):11531186, 2019.
- [33] M. Fornasier, B. Piccoli, and F. Rossi. Mean-field sparse optimal control. *Philos. Trans. Roy. Soc. A*, 372(2028):20130400, 2014.
- [34] M. Fornasier and F. Solombrino. Mean-field optimal control. *ESAIM Control Optim. Calc. Var.*, 20(4):11231152, 2014.
- [35] B. D. Goddard, A. Nold, and S. Kalliadasis. 2DChebClass [Software]. <http://dx.doi.org/10.7488/ds/1991>, 2017.
- [36] J.-P. Hansen and I. R. McDonald. *Theory of Simple Liquids: with Applications to Soft Matter*. Academic Press, 2013.
- [37] P. Hohenberg and W. Kohn. Inhomogeneous electron gas. *Phys. Rev.*, 136(3B):B864, 1964.
- [38] L. D. Landau and E. M. Lifshitz. *Statistical Physics: Vol. 5 (Course of Theoretical Physics)*. Butterworth-Heinemann, 3rd edition, 1980.
- [39] J.-M. Lasry and P.-L. Lions. Jeux à champ moyen. I - Le cas stationnaire. *Comptes Rendus*

- Math.*, 343(9):619–625, 2006.
- [40] J.-M. Lasry and P.-L. Lions. Jeux à champ moyen. II - Horizon fini et contrôle optimal. *Comptes Rendus Math.*, 343(10):679–684, 2006.
- [41] J.-M. Lasry and P.-L. Lions. Mean field games. *Cahiers de la Chaire Finance et Développement Durable*, 2007.
- [42] J.-M. Lasry and P.-L. Lions. Mean field games. *Jpn. J. Math.*, 2:229–260, 2007.
- [43] B. Leimkuhler and C. Matthews. *Molecular Dynamics*. Springer, 2016.
- [44] J. Lorenz. Continuous opinion dynamics under bounded confidence: A survey. *Internat. J. Modern Phys. C*, 18(12):1819–1838, 2007.
- [45] J. F. Lutsko. Recent developments in classical density functional theory. In S. A. Rice, editor, *Advances in Chemical Physics*, volume 144, pages 1–92. John Wiley & Sons, 2010.
- [46] J. F. Lutsko. A dynamical theory of nucleation for colloids and macromolecules. *J. Chem. Phys.*, 136(3):034509, 2012.
- [47] M. Huang, P. E. Caines, and R. P. Malhamé. Individual and mass behaviour in large population stochastic wireless power control problems: centralized and Nash equilibrium solutions. In *42nd IEEE International Conference on Decision and Control*, pages 98–103, Dec 2003.
- [48] U. M. B. Marconi and P. Tarazona. Dynamic density functional theory of fluids. *J. Chem. Phys.*, 110(16):8032–8044, 1999.
- [49] K.-A. Mardal, B. F. Nielsen, and M. Nordaas. Robust preconditioners for PDE-constrained optimization with limited observations. *BIT Numer. Math.*, 57:405–431, 2017.
- [50] J. Messer and H. Spohn. Statistical mechanics of the isothermal Lane–Emden equation. *J. Stat. Phys.*, 29(3):561–578, 1982.
- [51] A. Nold, B. D. Goddard, P. Yatsyshin, N. Savva, and S. Kalliadasis. Pseudospectral methods for density functional theory in bounded and unbounded domains. *J. Comput. Phys.*, 334:639–664, 2017.
- [52] J. W. Pearson and M. Stoll. Fast iterative solution of reaction–diffusion control problems arising from chemical processes. *SIAM J. Sci. Comput.*, 35(5):B987–B1009, 2013.
- [53] J. W. Pearson, M. Stoll, and A. J. Wathen. Regularization-robust preconditioners for time-dependent PDE-constrained optimization problems. *SIAM J. Matrix Anal. Appl.*, 33(4):1126–1152, 2012.
- [54] B. Piccoli, F. Rossi, and E. Trélat. Control to flocking of the kinetic Cucker–Smale model. *SIAM J. Math. Anal.*, 47(6):4685–4719, 2014.
- [55] R. Pinnau, C. Totzeck, O. Tse, and S. Martin. A consensus-based model for global optimization and its mean-field limit. *Math. Models Methods Appl. Sci.*, 27(1):183204, 2017.
- [56] M. J. D. Powell. A Fortran subroutine for solving systems of nonlinear algebraic equations. In P. Rabinowitz, editor, *Numerical Methods for Nonlinear Algebraic Equations*, chapter 7. Gordon and Breach, 1970.
- [57] T. Rees, H. S. Dollar, and A. J. Wathen. Optimal solvers for PDE-constrained optimization. *SIAM J. Sci. Comput.*, 32(2):271–298, 2010.
- [58] E. Roman and W. Dieterich. Classical fluid in a periodic potential and the density-functional approach. *Phys. Rev. A*, 32(6):3726, 1985.
- [59] R. Roth. Fundamental measure theory for hard-sphere mixtures: a review. *J. Phys. Condens. Matter*, 22(6):063102, 2010.
- [60] L. F. Shampine, M. W. Reichelt, and J. A. Kierzenka. Solving index-1 DAEs in MATLAB and Simulink. *SIAM Rev.*, 41(3):538–552, 1999.
- [61] M. Stoll and A. Wathen. All-at-once solution of time-dependent PDE-constrained optimization problems. Technical Report NA-10-13, University of Oxford, 2010.
- [62] G. Strang. On the construction and comparison of difference schemes. *SIAM J. Numer. Anal.*, 5(3):506–517, 1968.
- [63] A. Szabo and N. S. Ostlund. *Modern Quantum Chemistry: Introduction to Advanced Electronic Structure Theory*. Courier Corporation, 2012.
- [64] P. Tarazona, J. A. Cuesta, and Y. Martínez-Ratón. Density functional theories of hard particle systems. In *Theory and Simulation of Hard-Sphere Fluids and Related Systems*, pages 247–341. Springer, 2008.
- [65] L. N. Trefethen. *Spectral Methods in MATLAB*. SIAM, 2000.
- [66] F. Tröltzsch. *Optimal Control of Partial Differential Equations: Theory, Methods, and Applications*. American Mathematical Society, 2010.
- [67] G. A. Voth. *Coarse-Graining of Condensed Phase and Biomolecular Systems*. CRC Press, 2008.
- [68] J.-Z. Wu. Density functional theory for chemical engineering: From capillarity to soft materials. *AIChE J.*, 52(3):1169–1193, 2006.
- [69] J.-Z. Wu and Z.-D. Li. Density-functional theory for complex fluids. *Ann. Rev. Phys. Chem.*,

- 58:85–112, 2007.
- [70] C. A. Yates, R. E. Baker, R. Erban, and P. K. Maini. Refining self-propelled particle models for collective behaviour. *Can. Appl. Math. Q.*, 18(3):299–350, 2010.
- [71] W. Zulehner. Nonstandard norms and robust estimates for saddle point problems. *SIAM J. Matrix Anal. Appl.*, 32(2):536–560, 2011.